Dynamical theoretical model of the high-resolution double-crystal x-ray diffractometry of imperfect single crystals with microdefects

V. B. Molodkin, S. I. Olikhovskii, E. N. Kislovskii, T. P. Vladimirova, E. S. Skakunova, R. F. Seredenko, and B. V. Sheludchenko

G. V. Kurdyumov Institute for Metal Physics, NASU, Vernadsky Boulevard 36, 03680 Kyiv, Ukraine

(Received 29 July 2008; revised manuscript received 24 November 2008; published 30 December 2008)

The dynamical diffraction model has been developed for the quantitative description of rocking curves (RCs) measured in the Bragg diffraction geometry from single crystals containing homogeneously distributed microdefects of several types and with arbitrary sizes. The analytical expressions for coherent and diffuse RC components, which take self-consistently multiple-scattering effects into account and depend explicitly on microdefect characteristics (radius, concentration, strength, etc.), have been derived with taking into account the instrumental factors. The developed model has been applied to determine the characteristics of oxygen precipitates and dislocation loops in silicon crystals grown by Czochralsky and float-zone methods using RCs measured by the high-resolution double-crystal x-ray diffractometer. It has been shown, particularly, that completely dynamical consideration of Huang as well as Stockes-Wilson diffuse scattering (DS) in both diffuse RC component and coefficient of extinction of coherent RC component due to DS, together with taking asymmetry and thermal DS effects into account, provides the possibility to distinguish contributions into RC from defects of different types, which have equal or commensurable effective radii.

DOI: 10.1103/PhysRevB.78.224109 PACS number(s): 61.72.Dd

I. INTRODUCTION

Investigations of the diffuse scattering (DS) intensity distributions in the reciprocal-lattice space are widely used for the characterization of small defects (point defects and their clusters with nanometer sizes) in metals and alloys[1–10] and microdefects (new phase particles, dislocation loops, etc.) in semiconductors.[11–19] If point defects and small clusters with sizes of the order of lattice constant are investigated, the characteristic half widths of DS intensity distributions are comparable with distances between reciprocal-lattice points and can make in angular units from several up to tens of degrees. Therefore, the registration of corresponding rocking curves (RCs) can be provided by the usual double-crystal diffractometer (DCD) with resolution of few angular minutes. The interpretation of such measurements can successfully be carried out by using the kinematical diffraction theory.[20–23]

However, in the case of large microdefects which sizes are comparable with the extinction length Λ, the half widths of corresponding DS intensity distributions are commensurable with the half width of the Bragg peak, and then the analysis of diffraction patterns becomes more complicated because of the superposition of coherent and diffuse RC components within the total reflection range. Thus, it becomes necessary to give the self-consistent description of the behavior of coherent and diffuse components of the diffraction intensity and to account for dynamical scattering effects in DS intensity distributions.[24–28] It should be remarked, that for real single-crystalline materials, both as-grown and after various technological treatments, the problem appears often jet more complicated because of the simultaneous presence of microdefects of various types with wide spreads of sizes.[29,30]

The characteristic feature of DS intensity distributions in reciprocal-lattice space in the case of microdefects with an effective radius R_{eff} is the existence of two regions with the boundary between them, which corresponds to a momentum transfer $k \sim k_m = 1/R_{\mathrm{eff}}$.[20,21,27] The DS intensity decreases with increasing k as $I_{\mathrm{DS}} \sim 1/k^2$ at $k \ll k_m$ (Huang scattering region) and as $I_{\mathrm{DS}} \sim 1/k^4$ at $k \gg k_m$ (Stockes-Wilson scattering region). Consequently, the DS intensity is concentrated near a reciprocal-lattice point with increasing R_{eff}. When diffractometric investigations are carried out, the measured DS intensity is integrated, as rule, over one component of a momentum transfer $\mathbf{k}$ (over the vertical divergence in triple-crystal diffractometer) or over two components of $\mathbf{k}$ (over vertical and horizontal divergences of diffracted x-ray beam in DCD with widely open detector window). In consequence of such integrations, the dependence of the measured I_{DS} on k is changed, namely, exponents of k are decreased by integers 1 or 2, respectively. Nevertheless, the most important information on sizes, concentrations, and strengths of defects in measured angular DS intensity distributions is kept in both cases. In particular, after the two-dimensional integration of I_{DS}, which is performed at measurements by DCD with widely open detector window, the effective radius of defects R_{eff} can be determined from an intersection point of the linear segment of the integrated I_{DS} dependence on $\ln k$, which is continued up to an abscissa axis.[1,6,21] Practical realization of this simple method often fails because of large spreads of defect sizes and/or simultaneous presence of several defect types in the crystal under investigation. Such method becomes completely inapplicable when Bragg peak and DS intensity peak are superimposed, i.e., the Huang scattering region is located within in the total reflection range what takes place if the relation $R_{\mathrm{eff}} \geq \Lambda$ holds.

The aim of the present paper is to develop the most complete diffraction model for the adequate quantitative description of RCs measured at the Bragg diffraction geometry from single crystals which contain simultaneously microdefects of various types and arbitrary sizes. This model is based on the

generalized dynamical theory of x-ray diffraction by single crystals with randomly distributed microdefects[26,27] and takes self-consistently account for multiple-scattering processes in both coherent (Sec. II) and diffuse (Sec. III) components of the diffraction intensity measured by DCD with widely open detector window. The obtained analytical expressions for these components include both static Debye-Waller factor and absorption coefficients due to DS, which can be calculated at the simultaneous presence of several types of microdefects and possible existence of correlations between them.

The developed model has been applied to characterize the microdefect structures in silicon crystals grown by float-zone (FZ) and Czochralsky (Cz) methods using RCs measured by DCD with widely open detector window (see also Refs. 31 and 32). Instrumental function of the DCD is analyzed in Sec. IV, experimental details are described in Sec. V, and the treatment procedure and characterization results are discussed in Sec. VI. Short resume and conclusions are given in Sec. VII.

II. COHERENT COMPONENT OF ROCKING CURVE FROM AN IMPERFECT CRYSTAL

A. Coherent reflectivity

According to the generalized dynamical theory of x-ray scattering by imperfect single crystals with randomly distributed microdefects,[26,27] the coherent wave field in such crystals for each polarization state (σ and π) can be represented in two-beam approximation as sum of transmitted and diffracted waves,

$$D(\mathbf{r}) = D_T(\mathbf{r}) + D_S(\mathbf{r}), \tag{1}$$

$$D_T(\mathbf{r}) = \sum_{\delta} D_0^{\delta} e^{-i\mathbf{K}_0^{\delta}\mathbf{r}}, \quad D_S(\mathbf{r}) = \sum_{\delta} D_{\mathbf{H}}^{\delta} e^{-i\mathbf{K}_{\mathbf{H}}^{\delta}\mathbf{r}}, \tag{2}$$

where $\mathbf{r}$ is the space coordinate and $\delta=1,2$. The amplitudes of transmitted (D_0^{δ}) and diffracted ($D_{\mathbf{H}}^{\delta}$) coherent plane waves are described by expressions

$$D_0^{\delta} = (-1)^{\delta} E_0 \frac{B_{\delta'}}{B_1 - B_2}, \quad D_{\mathbf{H}}^{\delta} = c^{\delta} D_0^{\delta},$$

$$B_{\delta} = c^{\delta} e^{-iK\Delta_{\delta}t}, \quad c^{\delta} = -\frac{-2\gamma_0\Delta_{\delta} + \chi_0 + \Delta\chi_{00}^{\delta}}{CE\chi_{-\mathbf{H}} + \Delta\chi_{0\mathbf{H}}^{\delta}}, \tag{3}$$

where E_0 is the amplitude of an incident plane wave, t is the crystal thickness, and $\delta' \neq \delta$. Amplitudes of coherent wave fields are related with characteristics of the crystal defect structure via the static Debye-Waller factor $E=\exp(-L_H)$ and complex dispersion corrections due to DS $\Delta\chi_{\mathbf{GG}'}^{\delta}$ ($\mathbf{G}$ and $\mathbf{G}'=0$ or $\mathbf{H}$). Accommodations of wave vectors of strong Bragg waves $\mathbf{K}_{\mathbf{H}}^{\delta}=\mathbf{K}_0^{\delta}+\mathbf{H}$ and $\mathbf{K}_0^{\delta}=\mathbf{K}+K\Delta_{\delta}\mathbf{n}$ in Eq. (2) are described by the expression

$$\Delta_{\delta} = \frac{1}{2\gamma_0}(\chi_0 + \Delta\chi_{00}^{\delta}) + \frac{\lambda}{2\Lambda}[y + (-1)^{\delta}\sqrt{y^2-1}],$$

$$y = (\alpha - \alpha_0)\sqrt{b}/\sigma, \quad \sigma^2 = (CE\chi_{\mathbf{H}} + \Delta\chi_{\mathbf{H}0}^{\delta})(CE\chi_{-\mathbf{H}} + \Delta\chi_{\mathbf{H}0}^{\delta}),$$

$$\alpha = -\Delta\theta \sin 2\theta_B, \quad 2\alpha_0 = \chi_0 + \Delta\chi_{\mathbf{HH}}^{\delta} + (\chi_0 + \Delta\chi_{00}^{\delta})/b, \tag{4}$$

where $\mathbf{H}$ is the reciprocal-lattice vector, $\mathbf{n}$ is the inner normal to the entrance crystal surface, $\Lambda=\lambda\sqrt{\gamma_0|\gamma_H|}/\sigma$ is a complex extinction length, $K=2\pi/\lambda$ is the module of the wave vector $\mathbf{K}$ of an incident plane wave, λ is x-ray wavelength, C is the polarization factor equal to 1 or $\cos 2\theta_B$ for σ and π polarizations, respectively, θ_B is the Bragg angle, $\Delta\theta$ is an angular deviation of the investigated crystal from an exact Bragg position, $\chi_{\mathbf{G}}$ are Fourier components of the perfect-crystal polarizability ($\mathbf{G}=0,\pm\mathbf{H}$), $b=\gamma_0/|\gamma_H|$ is the parameter of diffraction asymmetry, and γ_0 and γ_H are direction cosines of wave vectors of incident ($\mathbf{K}$) and scattered ($\mathbf{K}'$) plane waves, respectively.

The amplitude of the diffracted plane wave in a vacuum $E_{\mathbf{H}}$, which is generated by the superposition of diffracted coherent plane waves in crystal $D_S(\mathbf{r})$, is obtained from the boundary condition on a crystal surface, and in the case of Bragg diffraction geometry one obtains the following expression for the amplitude reflectivity:

$$r = (\zeta b)^{-1/2}\frac{E_{\mathbf{H}}}{E_0} = (\zeta b)^{1/2}\frac{e^{iK\Delta_1 t} - e^{iK\Delta_2 t}}{c^2 e^{iK\Delta_1 t} - c^1 e^{iK\Delta_2 t}}, \tag{5}$$

where $\zeta=(CE\chi_{\mathbf{H}}+\Delta\chi_{\mathbf{H}0})(CE\chi_{-\mathbf{H}}+\Delta\chi_{0\mathbf{H}})^{-1}$ and E_0 and $E_{\mathbf{H}}$ are amplitudes of the incident and coherently scattered plane waves in a vacuum, respectively. The coherent component of the crystal reflectivity can be described then as

$$R_B(\mathbf{k}) = R_{\mathrm{coh}}(\Delta\theta,\varphi)\,\delta(\Delta\theta' - b\Delta\theta)\,\delta(\varphi' - \varphi), \tag{6}$$

$$R_{\mathrm{coh}}(\Delta\theta,\varphi) = |r|^2, \tag{7}$$

where $\delta(x)$ is Dirac's δ function, $\Delta\theta$ and $\Delta\theta'$ are angular deviations of wave vectors $\mathbf{K}$ and $\mathbf{K}'$ in the horizontal plane, i.e., the diffraction plane ($\mathbf{K},\mathbf{H}$), from corresponding exact Bragg directions, and φ and φ' are angular deviations of the same vectors in the vertical plane.

In x-ray diffraction investigations of structural imperfections of real single crystals by using measurements on DCD with widely open detector window, the diffracted intensity is integrated over an exit solid angle and the measured coherent RC component is described by Eq. (7). The information on structural imperfections and statistical characteristics of defects is involved in this component through the static Debye-Waller factor E and dispersion corrections due to DS $\Delta\chi_{\mathbf{GG}'}$. These diffraction parameters of structural perfection are obtained by statistical averaging of the functions dependent on random fields of static atom displacements that are caused by defects in a crystal lattice.[26,27]

B. Static Debye-Waller factor

The static Debye-Waller factor has the form

$$E = e^{-L_{\mathbf{H}}} = \langle e^{-i\mathbf{H}\mathbf{u}(\mathbf{r})}\rangle. \tag{8}$$

When microdefects of several types are present in a crystal, the field of static atom displacements in Eq. (8) can be written as[20]

$$\mathbf{u}(\mathbf{R}_s) = \sum_{\alpha} \sum_{t} (c_{\alpha t} - c_{\alpha}) \mathbf{U}_{\alpha}(\mathbf{R}_s - \mathbf{R}_t), \tag{9}$$

where $c_{\alpha t}=0$ and 1 are occupation numbers for α-type defects in a lattice point $\mathbf{R}_t$, $c_{\alpha}=\langle c_{\alpha t}\rangle$ is the concentration of α-type defects, and $\mathbf{U}_{\alpha}(\mathbf{R}_s-\mathbf{R}_t)$ is the static displacement of an atom in a lattice point $\mathbf{R}_s$, which is caused by α-type defect in a point $\mathbf{R}_t$. Equation (9) holds if the principle of the superposition of static atom displacements is valid, i.e., at small defect concentrations $c_{\alpha} \ll 1$. In general, there exists a correlation in relative positions of defects. It can be described by the correlation parameters, which, if only pair correlations are considered, are defined as

$$\varepsilon_{\alpha\alpha'}(\boldsymbol{\rho}) = \langle (c_{\alpha s} - c_{\alpha})(c_{\alpha' s'} - c_{\alpha'}) \rangle, \tag{10}$$

where $\boldsymbol{\rho}=\mathbf{R}_s-\mathbf{R}_{s'}$. If the method of cumulant expansions is used at averaging in Eq. (8), then one can obtain (cf. Ref. 20)

$$L_{\mathbf{H}} = \sum_{\alpha} L_{\mathbf{H}}^{\alpha} + \sum_{\alpha\alpha'} L_{\mathbf{H}}^{\alpha\alpha'}, \quad L_{\mathbf{H}}^{\alpha} = c_{\alpha} \sum_{\boldsymbol{\rho}} [1 - e^{i\mathbf{H}\mathbf{U}_{\alpha}(\boldsymbol{\rho})}],$$

$$L_{\mathbf{H}}^{\alpha\alpha'} = -\frac{1}{2} \sum_{\boldsymbol{\rho}' \neq \boldsymbol{\rho}} \varepsilon_{\alpha\alpha'}(\boldsymbol{\rho} - \boldsymbol{\rho}')[1 - e^{i\mathbf{H}\mathbf{U}_{\alpha}(\boldsymbol{\rho})}][1 - e^{i\mathbf{H}\mathbf{U}_{\alpha'}(\boldsymbol{\rho}')}]. \tag{11}$$

The first sum in the exponent of static Debye-Waller factor (11) contains contributions separately from each type of defects, and the second one describes contributions from pair correlations between defects of different types.

C. Coefficient of absorption due to diffuse scattering

The dispersion corrections due to DS can be subdivided into real and imaginary parts[27]

$$\Delta\chi_{\mathbf{GG}'} = P_{\mathbf{GG}'}^{\delta} - i\mu_{\mathbf{GG}'}^{\delta}/K, \tag{12}$$

The coefficients of absorption due to DS can be calculated in the first approximation of the dynamical perturbation theory developed in Refs. 26 and 27 as follows:

$$\mu_{\mathbf{GG}'}^{\delta}(\Delta\theta) = C^2K^2 \frac{V}{8\pi^2} \sum_{\tau=1,2} (-1)^{\tau} \mathrm{Re} \times \int_{K'=K_{0\mathbf{q}}^{\delta\tau}} dS_{\mathbf{K}'} f_{\mathbf{GG}'}(\mathbf{q}_{\delta\tau}) S_{\mathbf{GG}'}(-\mathbf{q}_{\delta\tau}), \tag{13}$$

where the integration at fixed δ is performed over two sheets of the dispersion surface for wave vectors $\mathbf{K}_{0\mathbf{q}}^{\delta t}$ of diffusely scattered plane waves, and the following notation was used:

$$f_{\mathbf{GG}'}(\mathbf{q}_{\delta\tau}) = a_{\mathbf{GG}'}^{\tau}[4\gamma_H(\Delta_2'^0 - \Delta_1'^0)]^{-1},$$

$$a_{\mathbf{GG}'}^{\tau} = -2\varepsilon_{\mathbf{Gq}}^{0\tau} + \chi_0, \quad a_{0\mathbf{H}}^{\tau} = CE\chi_{\mathbf{H}}, \quad a_{\mathbf{H}0}^{\tau} = CE\chi_{-\mathbf{H}}. \tag{14}$$

The wave vectors of diffusely scattered waves are complex due to complex momentum transfers $\mathbf{q}_{\delta\tau}$ from wave vectors of strong Bragg waves $\mathbf{K}_0^{\delta}$,

$$\mathbf{K}_{0\mathbf{q}}^{\delta\tau} = \mathbf{K}_0^{\delta} + \mathbf{q}_{\delta\tau}, \quad \mathbf{q}_{\delta\tau} = \mathbf{k} + K(\Delta_{\tau}'^0 - \Delta_{\delta}^0)\mathbf{n}. \tag{15}$$

The accommodations of wave vectors of diffusely scattered waves in Eq. (15) are described by the expression

$$\Delta_{\tau}'^0 = \frac{x_0}{2\gamma_0} + \frac{\lambda}{2\Lambda_0}[y_0' + (-1)^{\tau}\sqrt{y_0'^2 - 1}],$$

$$y_0' = (\alpha' - \alpha_0^0)\sqrt{b}/\sigma_0, \quad \alpha' = -\Delta\theta' \sin 2\theta_B,$$

where $\alpha_0^0=\frac{1}{2}\chi_0(1+b^{-1})$ and $\sigma_0=C^2E^2\chi_{\mathbf{H}}\chi_{-\mathbf{H}}$.

The correlation functions $S_{\mathbf{GG}'}(\mathbf{q})$ have appeared in Eq. (13) in consequence of replacing the products of fluctuating lattice sums by corresponding averages on the statistical ensemble of defects in a crystal lattice (so-called self-averaging),

$$S_{\mathbf{GG}'}(\mathbf{q}) = \langle \delta\chi_{\mathbf{q}-\mathbf{H}+2\mathbf{G}} \delta\chi_{-\mathbf{q}+\mathbf{H}-2\mathbf{G}'} \rangle, \tag{16}$$

where $\mathbf{G}$ and $\mathbf{G}'=0$ or $\mathbf{H}$, $\mathbf{q}$ is a complex momentum transfer, $\delta\chi_{\mathbf{G}+\mathbf{q}}$ is the Fourier component of the fluctuation part of the crystal polarizability, and angular brackets denote averaging on the statistical ensemble of defects.

As far as the behavior of the correlation functions in Eq. (13) is weakly changed with different δ and τ indices, one can approximately put

$$S_{\mathbf{GG}'}(\mathbf{q}_{\delta\tau}) \approx S(\mathbf{q}) = \mathrm{Re}\langle \delta\chi_{\mathbf{q}-\mathbf{H}+2\mathbf{G}} \delta\chi_{-\mathbf{q}+\mathbf{H}-2\mathbf{G}'} \rangle, \tag{17}$$

where $\mathbf{q}=\mathbf{k}+i\mu_i\mathbf{n}$ and μ_i is the limiting value of an interference absorption coefficient $\mu_i^{\delta\tau}=K\,\mathrm{Im}(\Delta_{\tau}'^0-\Delta_{\delta}^0)$ at $|\Delta\theta|$ and $|\Delta\theta'| \to \infty$. Then we can perform the approximate summation in Eq. (13) by using relations (14)–(17), and we can replace the integration over sheets of the dispersion surface by the integration over the plane tangent to Ewald sphere near the reciprocal-lattice point considered (see Fig. 1),

$$\mu_{00}(\Delta\theta) \approx b\frac{C^2V}{4\lambda^2} \int d\mathbf{k}' S(\mathbf{q}), \tag{18}$$

$$\mu_{\mathbf{HH}}(\Delta\theta) \approx b^{-1}\mu_{00}(\Delta\theta), \quad \mu_{0\mathbf{H}}(\Delta\theta) \approx \mu_{\mathbf{H}0}(\Delta\theta) \approx 0. \tag{19}$$

To calculate the correlation function $S(\mathbf{q})$, one can use the method of fluctuation waves of the defect concentration,[19] which provides at $c_{\alpha} \ll 1$ and $q \ll k_{m\alpha}=1/R_{\mathrm{eff}}^{\alpha}$ the approximate expression[33]

$$\delta\chi_{\mathbf{H}+\mathbf{q}} \approx iE\chi_{\mathbf{H}} \sum_{\alpha} (\mathbf{H}\mathbf{U}_{\alpha\mathbf{q}}) c_{\alpha\mathbf{q}}, \tag{20}$$

$$\mathbf{U}_{\alpha\mathbf{q}} = \frac{1}{v_c} \int d\mathbf{r} \mathbf{U}_{\alpha}(\mathbf{r}) e^{i\mathbf{q}\mathbf{r}}, \quad c_{\alpha\mathbf{q}} = \frac{1}{N} \sum_{t} (c_{\alpha t} - c_{\alpha}) e^{i\mathbf{q}\mathbf{R}_t}, \tag{21}$$

where v_c is the unit-cell volume and N is the number of unit cells in a crystal. If only pair correlations in defect distributions exist, the relation holds[19]

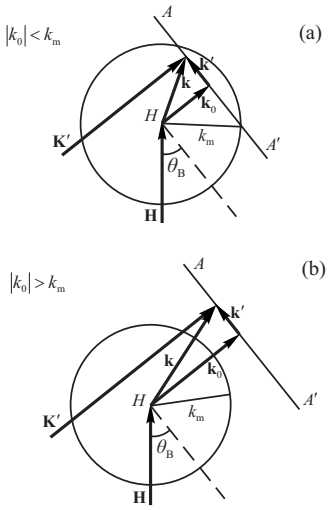

FIG. 1. Schematic plot of two cases of DS intensity integration in a momentum space, where **AA′** line represents the intersection of coherent scattering plane (**K**,**H**) with integration plane tangent to Ewald sphere: (a) $|\mathbf{k}_0| < k_m$, the integration interval includes both Huang ($k < k_m$) and Stokes-Wilson ($k > k_m$) scattering regions, (b) $|\mathbf{k}_0| > k_m$, the integration interval lies only in the Stokes-Wilson scattering region.

$$\langle c_{\alpha\mathbf{q}} c^*_{\alpha'\mathbf{q}} \rangle = \frac{1}{N}\left[\delta_{\alpha\alpha'} c_\alpha (1 - c_\alpha) + \sum_{\rho \neq 0} \varepsilon_{\alpha\alpha'}(\boldsymbol{\rho}) e^{i\mathbf{q}\boldsymbol{\rho}} \right], \quad (22)$$

where $\delta_{\alpha\alpha'}$ is Kronecker's symbol and $\varepsilon_{\alpha\alpha'}(\boldsymbol{\rho})$ are pair-correlation parameters. Then for the correlation function we obtain,

$$S(\mathbf{q}) = \sum_\alpha S_\alpha(\mathbf{q}) + \sum_{\alpha\alpha'} S_{\alpha\alpha'}(\mathbf{q}), \quad (23)$$

$$S_\alpha(\mathbf{q}) = \frac{c_\alpha}{N} E^2 \chi_{\mathbf{H}} \chi_{-\mathbf{H}} F^H_\alpha(\mathbf{q}), \quad F^H_\alpha(\mathbf{q}) = (\mathbf{H}\mathbf{U}_{\alpha\mathbf{q}})(\mathbf{H}\mathbf{U}_{\alpha-\mathbf{q}}), \quad (24)$$

$$S_{\alpha\alpha'}(\mathbf{q}) = \frac{1}{N} E^2 \chi_{\mathbf{H}} \chi_{-\mathbf{H}} \sum_{\boldsymbol{\rho} \neq 0} \varepsilon_{\alpha\alpha'}(\boldsymbol{\rho}) F^{H,H}_{\alpha\alpha'}(\mathbf{q}) e^{i\mathbf{q}\boldsymbol{\rho}},$$
$$F^{H,H}_{\alpha\alpha'}(\mathbf{q}) = (\mathbf{H}\mathbf{U}_{\alpha\mathbf{q}})(\mathbf{H}\mathbf{U}_{\alpha'-\mathbf{q}}). \quad (25)$$

The second sum in Eq. (23) takes the influence of pair correlations in defect distributions into account, and superscript H in Eqs. (24) and (25) denotes that these equations are valid only in the Huang scattering region, i.e., at $k \ll k_{m\alpha}$. When considering momentum transfers in the Stokes-Wilson scattering region, i.e., the region of asymptotic DS at $k \gg k_{m\alpha}$, one has to multiply each term in Eq. (23) by $k_{m\alpha}/q$ (see Refs. 27 and 34) and, corresponding, to replace functions $F^H_\alpha(\mathbf{q})$ and $F^{H,H}_{\alpha\alpha'}(\mathbf{q})$ in Eqs. (24) and (25) by following ones:

$$F^{\mathrm{SW}}_\alpha(\mathbf{q}) = F^H_\alpha(\mathbf{q}) k^2_{m\alpha}/q^2 \quad (26)$$

and

$$F^{\mathrm{SW}}_{\alpha\alpha'}(\mathbf{q}) = F^H_{\alpha\alpha'}(\mathbf{q}) k_{m\alpha} k_{m\alpha'}/q^2, \quad (27)$$

if $q \gg k_{m\alpha}$ and $q \gg k_{m\alpha'}$, or by

$$F^{H,\mathrm{SW}}_{\alpha\alpha'}(\mathbf{q}) = F^H_{\alpha\alpha'}(\mathbf{q}) k_{m\alpha'}/q, \quad (28)$$

if $q \ll k_{m\alpha}$ and $q \gg k_{m\alpha'}$.

The derived expressions for coefficients of absorption due to DS [Eqs. (18) and (19)] provide the possibility for performing, with the use of relations (23)–(28), the correct calculations of angular dependencies of absorption effects because of DS for strong Bragg waves in crystals with microdefects of arbitrary sizes. Real parts of the dispersion corrections due to DS (12) are of the same order of magnitude as the imaginary parts of Eqs. (18) and (19), and can be calculated through these imaginary parts by using known dispersion relations.[35]

III. DIFFUSE COMPONENT OF ROCKING CURVE FROM AN IMPERFECT CRYSTAL

A. Differential diffuse reflectivity

In order to calculate the diffuse component of the differential reflection power of the crystal, one has to average the absolute square of the DS amplitude over a random distribution of defects and to divide it by the incident intensity,

$$R_{\mathrm{DS}}(\mathbf{k}) = \frac{\langle |f_{\mathbf{H}}(\mathbf{K}', \mathbf{K})|^2 \rangle}{\gamma_0 S |E_0|^2}, \quad (29)$$

$$f_{\mathbf{H}}(\mathbf{K}', \mathbf{K}) = \sum_\delta \sum_{\mathbf{G}} D^\delta_{\mathbf{G}}(\Delta\theta) F^\delta_{\mathbf{HG}}(\mathbf{k}), \quad (30)$$

where the vector $\mathbf{k} = \mathbf{K}' - \mathbf{K} - \mathbf{H}$ is the deviation of the wave vector $\mathbf{K}'$ of diffusely scattered wave in a vacuum from the reciprocal-lattice point **H**, $\delta = 1$ and 2, $\mathbf{G} = 0$ and **H**, the corner brackets denote the averaging over a random distribution of defects, and S is the entrance crystal surface area. The partial amplitudes of the scattering of strong Bragg waves into the diffuse ones in Eq. (30) have the form

$$F^\delta_{\mathbf{HG}}(\mathbf{K}', \mathbf{K}) = \frac{VK^2}{4\pi(B'_1 - B'_2)} \sum_\tau (-1)^\tau M^{\delta\tau}_{\mathbf{HG}} e^{-iK\Delta'_\tau t}, \quad (31)$$

$$M^{\delta\tau}_{\mathbf{HG}} = c'^{(\tau)} M^{\delta\tau}_{0\mathbf{G}}, \quad M^{\delta\tau}_{0\mathbf{G}} = \xi' X_{0\mathbf{G}}(\mathbf{q}_{\delta\tau})/c'^{(\tau)} + X_{\mathbf{HG}}(\mathbf{q}_{\delta\tau}), \quad (32)$$

$$X_{\mathbf{GG}'}(\mathbf{q}) = C_{\mathbf{GG}'} \delta\chi_{\mathbf{G}-\mathbf{G}'+\mathbf{q}}, \quad B'_\tau = c'^{(\tau)} e^{-iK\Delta'_\tau t}, \quad (33)$$

where $\tau' \neq \tau = 1, 2$, $\xi' = (CE\chi_{\mathbf{H}} + \Delta\chi'^{\tau}_{\mathbf{H}0})(CE\chi_{-\mathbf{H}} + \Delta\chi'^{\tau}_{0\mathbf{H}})^{-1}$, $C_{\mathbf{GG}'} = 1$ at $\mathbf{G}' = \mathbf{G}$, and $C_{\mathbf{GG}'} = C$ at $\mathbf{G}' \neq \mathbf{G}$, Δ'_τ are accommodations of wave vectors of diffusely scattered waves.

Expression (30) can be simplified substantially when the approximation of the semi-infinite crystal is valid, i.e., at $\mu_0 t \gg 1$, where $\mu_0 = K|\chi_{i0}|$ is the photoelectric absorption coefficient. In such a case, only one quasi-Bloch wave is remained in the wave fields of both strong Bragg and diffusely scattered waves. It follows then approximately from Eqs. (31)–(33) that

$$R_{\mathrm{DS}}(\mathbf{k}) \approx \frac{1}{\gamma_0 S}\left(\frac{CVK^2}{4\pi}\right)^2 F_{\mathrm{dyn}}\langle|\delta\chi_{\mathbf{H}+\mathbf{q}}|^2\rangle, \tag{34}$$

where $F_{\mathrm{dyn}}(\Delta\theta)=|1-c^{\delta}|^2$. Diffuse reflectivity (34) can be rewritten through the correlation function according to Eqs. (17)–(19) using relations (20)–(22),

$$R_{\mathrm{DS}}(\mathbf{k}) \cong \frac{1}{\gamma_0 S}\left(\frac{CVK^2}{4\pi}\right)^2 F_{\mathrm{dyn}}(\Delta\theta)S(\mathbf{q})p(t), \tag{35}$$

$$p(t) = (1-e^{-2\mu_i t})/(2\mu_i t) \approx 1/(2\mu_i t). \tag{36}$$

The interference absorption coefficient μ_i can be estimated as $\mu_i \approx (1+b)\mu_0/(2\gamma_0)$ at $|y|, |y'| \gg 1$ and $\mu_i \sim \pi/\Lambda$ at $|y|, |y'| \leq 1$, i.e., it describes the extinction effect for diffusely scattered waves. The factor F_{dyn} describes the angular modulation of DS intensity, which is caused by the dynamical interference of strong Bragg waves.

The integration of Eq. (35) over the Ewald sphere ($K'=K$) near the reciprocal-lattice point H with account for Eqs. (18) and (19) gives the "integral" diffuse component of the reflection coefficient measured by DCD with widely open detector window

$$R_{\mathrm{diff}}(\Delta\theta)\int_{K'=K} R_{\mathrm{DS}}(\mathbf{k})d\Omega_{\mathbf{K}'} = F_{\mathrm{dyn}}(\Delta\theta)\mu_{\mathbf{HH}}(\Delta\theta)p(t)t/\gamma_0, \tag{37}$$

where $d\Omega_{\mathbf{K}'}$ is a solid angle in $\mathbf{K}'$ direction and $dS_{\mathbf{K}'}=K^2 d\Omega_{\mathbf{K}'}$ is an element of surface area in the reciprocal space. It should be emphasized here that DS intensity integrated over exit angles at fixed orientation $\Delta\theta$ of the incident wave vector $\mathbf{K}$ [Eq. (37)] appears to be proportional to the coefficient of absorption of coherent waves due to DS (19) at the same angular deviation. The index δ in the factor F_{dyn} as well as indices δ and τ in the coefficient μ_i are fixed numbers of the remained wave fields, which values 1 or 2 depend on signs of angular deviations $\Delta\theta$ and $\Delta\theta'$, respectively.

B. Microdefect models

To obtain the analytical expression for the "integral" diffuse reflectivity (37) one should specify microdefect types with corresponding Fourier components of static displacement fields, which determine correlation functions in Eqs. (24) and (25). For two types of microdefects, namely, spherically symmetric clusters and randomly oriented prismatic dislocation loops, the functions $F_{\alpha}^{\mathbf{H}}(\mathbf{q})$ in Huang scattering region, if only the symmetrical part of DS intensity is considered, can be represented in a unified form as[33]

$$F_{\alpha}^{H}(\mathbf{q}) = H^2\left(B_1^{\alpha} + B_2^{\alpha}\left|\frac{\mathbf{H}_0\mathbf{q}}{q}\right|^2\right)\frac{1}{|\mathbf{q}|^2}, \tag{38}$$

where $\mathbf{H}_0=\mathbf{H}/H$ is the unit vector.

For the most simple model of spherical clusters ($\alpha=1$) one should put in Eq. (38)

$$B_1^1 = 0, \quad B_2^1 = (4\pi A_C/\upsilon_c)^2,$$

$$A_C = \Gamma\varepsilon R_C^3, \quad \Gamma = \frac{1}{3}\frac{(1+\nu)}{(1-\nu)}, \tag{39}$$

where A_C is the cluster strength, ν is the Poisson ratio, ε is the strain at the cluster interface, and R_C is the cluster radius. In the more complicated model of clusters with lower symmetry (e.g., platelike, ellipsoidal, or disk-shaped new phase particles lying in {100} planes of a cubic crystal), one can put approximately $B_1^1 \approx B_2^1 = (4\pi A_C/\nu_c)^2$ and $A_C = \frac{3}{4}\Gamma\varepsilon V_C/\pi$, where V_C is a cluster volume.

For the model of randomly oriented prismatic dislocation loops ($\alpha=2$) one should put in Eq. (38) after averaging over all continuous orientations of Burgers vectors

$$B_1^2 = \frac{4}{15}(\pi b R_L^2/\upsilon_c)^2, \quad B_2^2 = \beta B_1^2,$$

$$\beta = \frac{1}{4}(3\nu^2 + 6\nu - 1)/(1-\nu)^2, \tag{40}$$

where b is the modulus of Burgers vector and R_L is the dislocation loop radius. For the description of the antisymmetrical part of DS intensity in Huang scattering region, the corresponding term should be added to Eq. (38) (cf. Refs. 6, 20, and 21), namely,

$$\tilde{F}_{\alpha}^{H}(\mathbf{q}) = H\frac{B_3^{\alpha}}{q}, \quad B_3^{\alpha} = 2L_{\mathbf{H}}^{\alpha}\sqrt{B^{\alpha}}/c_{\alpha}, \tag{41}$$

where one can put approximately $B^1=B_2^1$ for clusters, and $B^2=B_1^2$ for dislocation loops.

For each type of microdefects also the proper value of the boundary between Huang and Stockes-Wilson scattering regions $k_{m\alpha}=1/R_{\mathrm{eff}}^{\alpha}$ should be chosen. By putting effective radii to be equal $R_{\mathrm{eff}}^1=\sqrt{H|A_C|}E$ for clusters and $R_{\mathrm{eff}}^2=R_L\sqrt{HbE}$ for dislocation loops we provide the correct description of asymptotic DS intensity with respect to both momentum transfer $\mathbf{q}$ and such parameters as H, b, and A_C.[20] Due to this choice of $k_{m\alpha}$, also the physically reasonable matching of Eqs. (24) and (26) at $k=k_{m\alpha}$ is provided.

C. Thermal diffuse scattering

In general, the DS intensity from microdefects is localized near reciprocal-lattice points where it is, as rule, significantly larger in comparison with the contribution of thermal DS in these regions, and for this reason the later one can be neglected at the analysis of measured diffraction patterns. However, at high reflection indices, the thermal DS intensity can be comparable with DS intensity from small microdefects and, therefore, should be taken into account to provide the correct quantitative interpretation of diffraction profiles.

In the case of thermal DS ($\alpha=3$), the Fourier component of the field of dynamic atom displacements from an oscillating atom in a single atom crystal can be considered in a harmonic approximation[20] according to which the function $F_3^H(\mathbf{q})$ has the form

$$F_3^H(\mathbf{q}) = \frac{\hbar H^2}{6m}\sum_{\rho=1}^{3}\frac{2n_{\mathbf{q}\rho}+1}{\omega_{\mathbf{q}\rho}},$$

$$n_{\mathbf{q}\rho} = [\exp(\hbar\omega_{\mathbf{q}\rho}/k_B T) - 1]^{-1}, \tag{42}$$

where $\hbar$ is Planck's constant, m is an atom mass, $\omega_{\mathbf{q}\rho}$ is the phonon frequency, and the summation is carried out over phonon polarizations. When considering thermal DS intensity in a close vicinity of a reciprocal-lattice point, the relation holds $\hbar\omega_{\mathbf{q}\rho}/k_B T \ll 1$, and therefore, one can put $n_{\mathbf{q}\rho} \approx k_B T/\hbar\omega_{\mathbf{q}\rho}$ and, consequently,

$$F_3^H(\mathbf{q}) \approx \frac{H^2}{m}\frac{k_B T}{\omega_{\mathbf{q}}^2}. \tag{43}$$

Phonon frequency in Eq. (43) can be calculated as $\omega_{\mathbf{q}} = v_S q$, where v_S is a phonon velocity which can be expressed through elastic constants and crystal density as $v_S = [\frac{1}{3}(C_{11} + 2C_{22} + 4C_{44})/\rho]^{1/2}$.[36] Expression (43) can be considered then as a particular case of Eq. (38) with the coefficients $B_1^3 = k_B T/(m v_S^2)$, $B_2^3 = 0$, and $B_3^3 = 0$.

It should be remarked here that the contribution from the Compton scattering in a double-crystal diffraction geometry with widely open detector window may be of the order of magnitude as that from thermal DS and should be taken into account as well. However, when performing the investigations of microdefect structures with atom clusters ranging in sizes from ten nanometers to larger ones, the contribution of the thermal DS in all the angular ranges measured is rather negligible, as will be shown below (Sec. VI), and, consequently, both thermal DS and Compton scattering contributions can be ignored when fitting relevant experimental RCs. For this reason, we do not consider here Compton scattering but retain the thermal DS description to check contributions of such kind processes.

D. "Integrated" diffuse reflectivity

The derivation of the analytical expression for the "integral" diffuse component of crystal reflectivity (37) is reduced to the integration in Eq. (18) for the coefficient of absorption due to DS. After the integration in Eq. (18) we obtain according to Eqs. (19) and (24)–(28)

$$\mu_{\mathbf{HH}}(\Delta\theta) = \sum_{\alpha} \mu_{\mathrm{DS}}^{\alpha}(k_0) + \sum_{\alpha\alpha'} \mu_{\mathrm{DS}}^{\alpha\alpha'}(k_0). \tag{44}$$

The absorption coefficient due to DS for microdefects of α type is described in Eq. (44) by the expression

$$\mu_{\mathrm{DS}}^{\alpha}(k_0) = c_\alpha C^2 E^2 m_0 J^{\alpha}(k_0), \tag{45}$$

$$m_0 = \frac{1}{4}\pi v_c H(H|\chi_{r\mathbf{H}}|\lambda)^2, \tag{46}$$

$$J^{\alpha}(k_0) = \frac{1}{\pi}\int d\mathbf{k}' F_\alpha(\mathbf{q}). \tag{47}$$

The correlation absorption coefficient due to DS in Eq. (44) has the form

$$\mu_{\mathrm{DS}}^{\alpha\alpha'}(k_0) = C^2 E^2 m_0 \sum_{\boldsymbol{\rho}} \varepsilon_{\alpha\alpha'}(\boldsymbol{\rho}) J^{\alpha\alpha'}(k_0) e^{i\mathbf{k}_0\boldsymbol{\rho}}, \tag{48}$$

$$J^{\alpha\alpha'}(k_0) = \frac{1}{\pi}\int d\mathbf{k}' F_{\alpha\alpha'}(\mathbf{q}) e^{i\mathbf{k}'\boldsymbol{\rho}}, \tag{49}$$

Functions F_α and $F_{\alpha\alpha'}$ in Eqs. (47) and (49) are described by Eqs. (24)–(28).

The further consideration will be restricted to the calculation of only absorption coefficients due to DS (45)–(47) and corresponding integral diffuse reflectivity (37). To perform the integration in Eq. (47), one should decompose a momentum transfer $\mathbf{k}$ into the components parallel ($\mathbf{k}_0$) and perpendicular ($\mathbf{k}'$) to the wave vector $\mathbf{K}'$ (see Fig. 1). Then relations $\mathbf{k} = \mathbf{k}_0 + \mathbf{k}'$ and $|\mathbf{q}|^2 = k'^2 + k_0^2 + \mu_i^2$ hold, and the integration can be performed in the polar coordinate system chosen in the plane tangent to the Ewald sphere near the reciprocal-lattice point H, in which the vector $\mathbf{k}'$ can be represented as $\mathbf{k}' = k'(\cos\varphi, \sin\varphi)$. When integrating over k' in Eq. (47), expression (38) for $F_\alpha^H(\mathbf{q})$ is used in the Huang scattering region ($0 \le k'^2 + k_0^2 \le k_m^2$), and this expression multiplied by $k_m^2/|\mathbf{q}|^2$ is substituted as $F_\alpha^{\mathrm{SW}}(\mathbf{q})$ into Eq. (47) in the Stockes-Wilson scattering region ($k'^2 + k_0^2 \ge k_m^2$). Also, the dependence of the interference absorption coefficient μ_i on exit angles $\Delta\theta'$ is neglected because its influence is smoothed due to integration, and thus, μ_i in Eq. (47) can be replaced by its limiting value at $|y'| \gg 1$

$$\mu_i \to \mu = \frac{\mu_0}{2\gamma_0}\frac{1+b}{2}\left(1 + \frac{r_i}{|g|}E\right), \tag{50}$$

$$r_i = \sqrt{\frac{1}{2}(\sqrt{u^2+v^2} - u)}, \quad u = (z^2 - g^2)E^{-2} + æ^2 - 1, \quad v = 2(zgE^{-2} - p), \tag{51}$$

$$z = \frac{\Delta\theta \sin 2\theta_B}{C|\chi_{r\mathbf{H}}|}\sqrt{b}, \quad g = -|\chi_{i0}|\frac{1+b^{-1}}{2C|\chi_{r\mathbf{H}}|}\sqrt{b}, \quad æ = \frac{|\chi_{i\mathbf{H}}|}{|\chi_{r\mathbf{H}}|}, \tag{52}$$

where $p = \pm æ$ for centrosymmetric crystals. The integration in Eq. (47) then can easily be performed, and with account for the angular aperture of the detector $\Delta\theta_a$ we obtain

$$J^{\alpha}(k_0) = \begin{cases} J_H^{\alpha}(k_0) + J_{H\text{-SW}}^{\alpha}(k_0) + \tilde{J}_H^{\alpha}(k_0) & \text{at } |k_0| \le k_{m\alpha} \\ J_{\mathrm{SW}}^{\alpha}(k_0) & \text{at } |k_0| \ge k_{m\alpha}, \end{cases} \tag{53}$$

where $k_0 = K\Delta\theta \sin 2\theta_B$. The angular dependence of the integral DS intensity in the Huang scattering region is described by symmetric and antisymmetric ($\tilde{J}_H^{\alpha}$) components in Eq. (53) as follows:

$$J_H^{\alpha}(k_0) = \frac{1}{2\pi}\int_0^{2\pi} d\varphi \int_0^{k_{m\alpha}^2 - k_0^2} dk'^2 F_\alpha^H(\mathbf{q}) = b_2 \ln\frac{k_{m\alpha}^2 + \mu^2}{k_0^2 + \mu^2} + (b_3 k_0^2 + b_4\mu^2)\left(\frac{1}{k_{m\alpha}^2 + \mu^2} - \frac{1}{k_0^2 + \mu^2}\right), \tag{54}$$

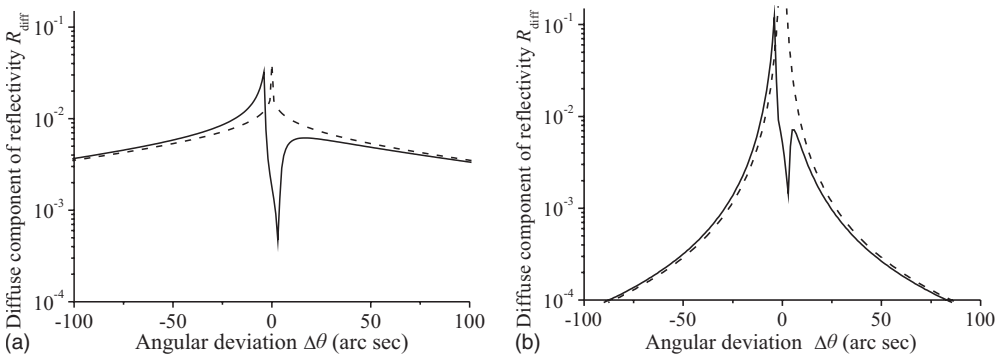

FIG. 2. Diffuse component of the reflectivity of Si crystal for (111) reflection of Cu $K\alpha 1$ radiation near the total reflection range in the cases of (a) small and (b) large dislocation loops with radii R_L=0.1 and 10 μm, respectively. The calculations according to dynamical and kinematical theories are shown by solid and dashed lines, respectively.

$$J^{\alpha}_{H\text{-SW}}(k_0) = \frac{1}{2\pi}\int_0^{2\pi} d\varphi \int_{k_{m\alpha}^2-k_0^2}^{k_a^2} dk'^2 F^{\text{SW}}_{\alpha}(\mathbf{q})$$
$$= \frac{k_{m\alpha}^2(k_a^2+k_0^2-k_{m\alpha}^2)}{(k_{m\alpha}^2+\mu^2)(k_a^2+k_0^2+\mu^2)}\left(b_2+\frac{1}{2}\right.$$
$$\left.\times\frac{(b_3k_0^2+b_4\mu^2)[(k_{m\alpha}^2+\mu^2)^2-(k_a^2+k_0^2+\mu^2)^2]}{(k_{m\alpha}^2+\mu^2)(k_a^2+k_0^2+\mu^2)(k_a^2+k_0^2-k_{m\alpha}^2)}\right), \tag{55}$$

$$\tilde{J}^{\alpha}_{H}(k_0) = \frac{1}{2\pi}\int_0^{2\pi} d\varphi \int_0^{k_{m\alpha}^2-k_0^2} dk'^2 \tilde{F}^{H}_{\alpha}(\mathbf{q}) = b_1(\sqrt{k_{m\alpha}^2+\mu^2}$$
$$-\sqrt{k_0^2+\mu^2}), \tag{56}$$

where $k_a = K\Delta\theta_a$ was supposed to be always larger in comparison with $k_{m\alpha}$. In the Stockes-Wilson scattering region the DS intensity profile is described by the expression

$$J^{\alpha}_{\text{SW}}(k_0) = \frac{1}{2\pi}\int_0^{2\pi} d\varphi \int_0^{k_a^2} dk'^2 F^{\text{SW}}_{\alpha}(\mathbf{q})$$
$$= \frac{k_{m\alpha}^2 k_a^2}{(k_0^2+\mu^2)(k_a^2+k_0^2+\mu^2)}\left\{b_2+\frac{1}{2}\right.$$
$$\left.\times\frac{(b_3k_0^2+b_4\mu^2)[(k_0^2+\mu^2)^2-(k_a^2+k_0^2+\mu^2)^2]}{k_a^2(k_0^2+\mu^2)(k_a^2+k_0^2+\mu^2)}\right\}. \tag{57}$$

The coefficients $b_i(i=\overline{1,4})$ in Eqs. (54)–(57) are connected with characteristics of microdefects by relations

$$b_1 = \frac{4L^{\alpha}_{\mathbf{H}}\sqrt{B_{2\alpha}}}{c_{\alpha}H}, \quad b_2 = B_{1\alpha}+\frac{1}{2}B_{2\alpha}\cos^2\theta_B,$$

$$b_3 = B_{2\alpha}\left(\frac{1}{2}\cos^2\theta_B - \sin^2\theta_B\right),$$

$$b_4 = B_{2\alpha}\left(\frac{1}{2}\cos^2\theta_B - \cos^2\psi\right),$$

where ψ is an angle of deviation of the diffraction plane from the crystal surface. If the inequality $k_a \gg k_{m\alpha}$ holds, we can put $k_a \to \infty$ in Eqs. (55) and (57), which are simplified then as follows:

$$J^{\alpha}_{H\text{-}SW}(k_0) = \frac{k_{m\alpha}^2}{k_{m\alpha}^2+\mu^2}\left(b_2-\frac{1}{2}\frac{b_3k_0^2+b_4\mu^2}{k_{m\alpha}^2+\mu^2}\right), \tag{58}$$

$$J^{\alpha}_{SW}(k_0) = \frac{k_{m\alpha}^2}{k_0^2+\mu^2}\left(b_2-\frac{1}{2}\frac{b_3k_0^2+b_4\mu^2}{k_0^2+\mu^2}\right). \tag{59}$$

Thus, we obtain in the approximation of semi-infinite crystal ($\mu_0 t \gg 1$) according to Eq. (37) the following expression for the diffuse component of RC measured by DCD with widely open detector window:

$$R_{\text{diff}}(\Delta\theta) \cong F_{\text{dyn}}(\Delta\theta)\frac{\mu_{\mathbf{HH}}(\Delta\theta)}{2\gamma_0\mu(\Delta\theta)}. \tag{60}$$

Expression (60) is very similar to the kinematical one,[6] and can be reduced to that by putting $F_{\text{dyn}}=1$, $\mu=\mu_0/\gamma_0$ in denominator, and $\mu=0$ in $\mu_{\mathbf{HH}}$ in nominator of Eq. (60),

$$R^{\text{kin}}_{\text{diff}}(\Delta\theta) \cong \frac{\mu^{\text{kin}}_{\text{HH}}(\Delta\theta)}{2\mu_0}. \tag{61}$$

Kinematical formula (61) is significantly simpler for performing numerical calculations as compared with Eq. (60) but has some serious limitations in the practical usage. Particularly, the logarithmic divergence exists in Eq. (61) at angular deviations $\Delta\theta \to 0$ and, consequently, at $k_0 \to 0$. To avoid this divergence, the cut-off parameter $k_c \sim 1/\Lambda$ in a momentum space, Λ being an extinction length, has been introduced artificially.[21] In dynamical expression (60) this divergence is removed in a natural way due to the interference absorption parameter μ, which has the order of magnitude of k_c within the total reflection range.

Also the restriction on the maximal allowable effective radius of microdefects $R_{\text{eff}} < \Lambda$, which was imposed implicitly in the derivation of the kinematical formula, is absent in Eq. (60), thus, providing the possibility to describe quantitatively in explicit analytical terms the Huang DS intensity also in the total reflection range at R_{eff} exceeding an extinction length. Besides, it should be remarked the importance of taking into account the detector entrance aperture to perform the correct quantitative characterization of crystal imperfec-

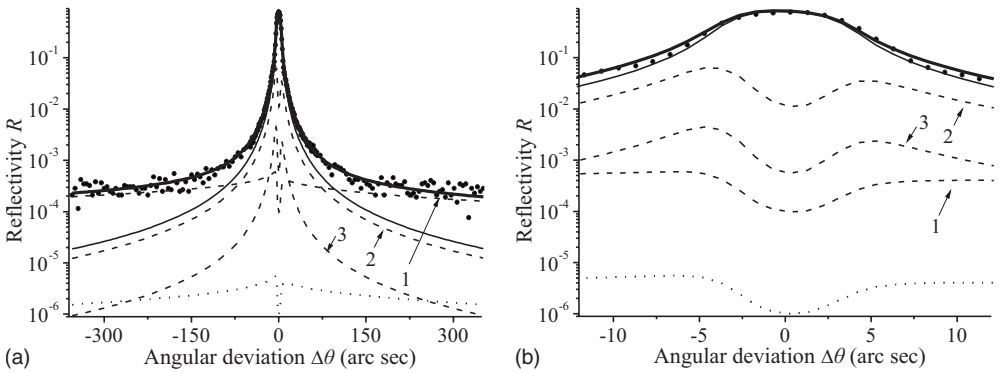

FIG. 3. RC of FZ Si sample for (111) reflection of Cu $K\alpha 1$ radiation (a) in the whole angular range measured and (b) in the total reflection range. The calculated total RC and its coherent component are shown by thick and thin solid lines, respectively. The contributions to the diffuse component of RC from dislocation loops with different sizes are shown by numerated broken lines, and thermal DS component is shown by a dotted line.

tions, especially, when effective radii of microdefects are so small that the relation $k_{m\alpha} \geq k_a$ holds.

The lower limit of the angular region, where a much more simple kinematical theory is sufficient for the adequate DS intensity analysis, is determined by the width of the total reflection range (nearly $1/\Lambda$ in a momentum space, Λ being an extinction length) and should be of the order of $10/\Lambda$. For this reason, of outstanding importance in the analysis is the value of the half width of DS intensity distribution for microdefects in the crystal under investigation, which is determined by the largest effective radius R_{eff} of the microdefects. If R_{eff} is significantly smaller in comparison with Λ, the kinematical approach will be sufficient for the correct description of the diffuse component, but for R_{eff} of the order of Λ or larger the account for dynamical effects becomes necessary (see Fig. 2). Particularly, the only dynamical approach can give the correct quantitative description of DS intensity distribution from microdefects with R_{eff} significantly larger than Λ [Fig. 2(c)].

On the other hand, it should be remarked that in the cases where dynamical effects are small, i.e., the scattering is predominantly kinematical, the use of the dynamical formulas remains useful as they automatically give a correct description of the kinematical scattering patterns. Moreover, if the dynamical approach is applied, it is not necessary to analyze and justify its validity for each specific experimental situation, what is required for the application of the kinematical theory.

IV. INSTRUMENTAL FUNCTION OF DOUBLE-CRYSTAL DIFFRACTOMETER

The dynamical theory of the integral DS measured by DCD, which has been stated above, provides the possibility for x-ray diffractometric characterization of complicated defect structures in real crystals including those with microdefects commensurable with an extinction length. In such cases, however, both coherent component of RC and instrumental resolution function of DCD should be taken into account to perform correct quantitative characterization of whole defect size spectrum.

X-ray intensity reflected by the investigated sample in the high-resolution DCD with parallel (+) or antiparallel (−) settings of the investigated sample with respect to the last reflection in the monochromator system can be represented as the convolution of reflection coefficients of all the crystals in the x-ray optical scheme,[37–39]

$$P_{\pm}(\Delta\theta) = \int_{\lambda_0-\Delta\lambda}^{\lambda_0+\Delta\lambda} d\lambda I(\lambda) \int_{-\varphi_m}^{\varphi_m} d\varphi \int_{-x_m}^{x_m} dx G(x,\varphi) R_1^{n_1}(x-\Phi_1) \times R_2^{n_2}(-x-\Phi_2) R_S[\pm(\Delta\theta - x) - \Phi_3], \quad (62)$$

where $2\Delta\lambda$, $2\varphi_m$, and $2x_m$ are intervals of the integration over wavelength, vertical, and horizontal divergences, respectively, the function $G(x,\varphi)$ describes the angular distribution of incident x-ray beam, n_1 and n_2 are reflection multiplicities at first and second monochromator crystals with

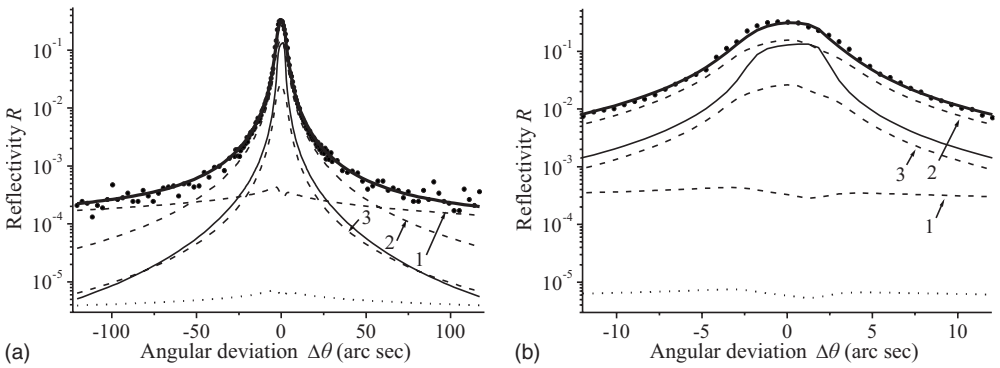

FIG. 4. See caption to Fig. 3, reflection Si (333).

TABLE I. Radii R_L and number densities $n_L=c_L/v_c$ of perfect dislocation loops in FZ Si sample.

hkl	*i* [a]	R_L (nm)	n_L (cm^{-3})	R (%)	R_w (%)
111	1	1	3.0×10^{17}	7	15
	2	5×10^2	1.0×10^{10}		
	3	1×10^4	4.0×10^3		
333	1	1	1.0×10^{17}	10	13
	2	5×10^2	1.5×10^{10}		
	3	1×10^4	4.0×10^3		

[a] *i* numerates populations of dislocation loops with different sizes.

reflectivities R_1 and R_2, respectively, and R_S is the reflectivity of the sample. The function $I(\lambda)$ in Eq. (62) describes the line shape of characteristic x-ray radiation with wavelength λ_0 and line half width w_λ

$$I(\lambda) = I_0/[1 + 4(\lambda - \lambda_0)/w_\lambda^2], \tag{63}$$

where I_0 is the incidence intensity, and also the notation was used

$$\Phi_i = \left(\frac{1}{2}\varphi^2 + \frac{\lambda - \lambda_0}{\lambda_0}\right) tg\,\theta_B^i \tag{64}$$

with θ_B^i being the Bragg angle of ith crystal.

After introducing the integration variable $u = \mp x - \Phi_3$ integral (62) can be reduced to the one fold convolution if the condition $\max \Phi_3(\varphi,\lambda) \ll x_m$ holds,

$$P_\pm(\Delta\theta) = \int_{\mp x_m}^{\pm x_m} du V_\pm(u) R_S(u \pm \Delta\theta), \tag{65}$$

where the instrumental function of DCD has the form

$$V_\pm(u) = \int_{\lambda_0-\Delta\lambda}^{\lambda_0+\Delta\lambda} d\lambda I(\lambda) \int_{-\varphi_m}^{\varphi_m} d\varphi R_1^{n_1}[\mp(u + \Phi_3) - \Phi_1] R_2^{n_2}[\pm(u + \Phi_3) - \Phi_2], \tag{66}$$

and it was supposed that $G(x,\varphi) \approx 1$. Then we have for RC of the sample under investigation, which was measured using nonpolarized radiation,

$$R(\Delta\theta) = \frac{P^{(\sigma)}(\Delta\theta) + P^{(\pi)}(\Delta\theta)}{P_0^{(\sigma)} + P_0^{\pi}}, \tag{67}$$

where $P_0^{\sigma,\pi} = \int_{-\infty}^{\infty} du V^{\sigma,\pi}(u)$ for σ and π components of the radiation.

The comparative calculations, which have been carried out by using exact formula (62) and approximate one [Eq. (65)] for the measurement scheme used, have shown that discrepancies between them do not exceed 3% in central part and 5% at "tails" of RC. Consequently, the simplified Eqs. (65) and (66) can be used in fitting procedures to decrease the calculation time.

V. EXPERIMENTAL SETUP AND SAMPLES

Experimental RCs of investigated silicon samples have been measured by using the high-resolution four-circle x-ray DCD with Cu tube and two flat Ge monochromators in the antiparallel setting. The symmetric (111) and (333) reflections were used at the samples under investigation, which were in the parallel setting relatively to the last reflection of the collimator, and the symmetric (333) reflection was used in both monochromators. The samples were rotated around a vertical axis by a step motor controlled by computer in steps of 1.0 and 0.6 arc sec for (111) and (333) reflections, respectively.

The investigated FZ Si sample having sizes 3×2 cm^2 has been cut from the central part of silicon single-crystal plate with a diameter 10 cm, which has been grown by a float-zone method. The sample thickness after lapping and chemomechanical polishing was about 525 μm, and then the sample was etched additionally to the depth about 10 μm. The conventional x-ray topography and scanning electron microscopy have not revealed any defects in the sample.

The Cz Si sample has been prepared by using wafer cut from the central part of Czochralsky-grown silicon ingot with growth axis [111]. The material was of *p*-type conductivity, its resistivity was 10.5 Ω cm. Concentrations of oxygen and carbon impurities were nearly 1.1×10^{18} and $\leq10^{17}$ cm^{-3}, respectively. The sample cut from the wafer perpendicularly to the growth axis was polished chemodynamically and then etched to the depth of 10 μm on both sides. Thermal annealing of the sample was performed at 750 °C for 30 h in a sealed-off quartz tube in the argon atmosphere at a pressure of 150 kPa to exclude possible oxygen "depletion" of the near-surface layer.

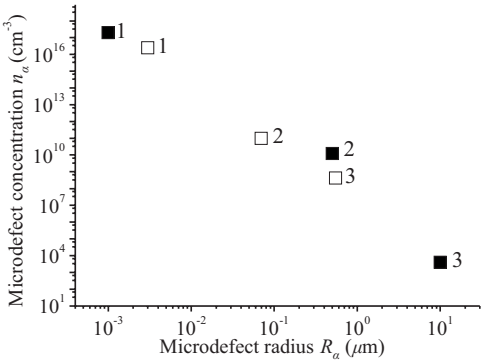

FIG. 5. Size distributions of dislocation loops in FZ Si sample $n_L(R_L)$ and oxygen precipitates in Cz Si sample $n_C(R_C)$ (black and white squares, respectively). Numbers at markers correspond to numbered RC components in Figs. 3, 4, 6, and 7.

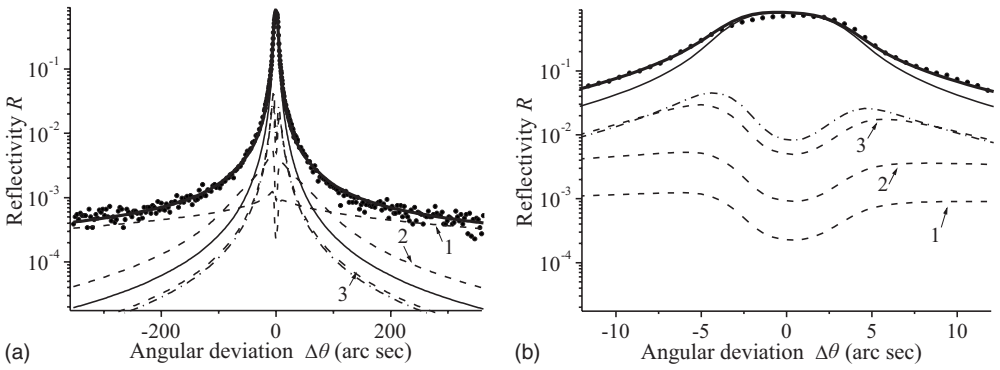

FIG. 6. RC of Cz Si sample for (111) reflection of Cu $K\alpha 1$ radiation (a) in the whole angular range measured and (b) in the total reflection range. The calculated total RC and its coherent component are shown by thick and thin solid lines, respectively. The contributions to the diffuse component of RC from oxygen precipitates with different sizes are shown by numerated broken lines, and one from dislocation loops is shown by a dashed-dotted line.

VI. ANALYSIS OF MEASURED ROCKING CURVES

The statistical treatment of RCs measured from FZ Si sample (Figs. 3 and 4) was carried out independently for (111) and (333) reflections of the characteristic Cu $K\alpha$ radiation. It was supposed in the defect model chosen that only perfect dislocation loops of the interstitial type are present in the investigated crystal.[40–44] However, all the attempts to describe the measured RCs in the whole angular range by varying only one dislocation loop radius and number density have appeared unsuccessful because the attempts allowed the acceptable fit only in local angular ranges of the RCs. The most probable cause of such difficulties may be the wide spread of dislocation loop radii, which leads to corresponding different DS intensity dependencies in different angular ranges.

Indeed, already by varying two sufficiently distinct dislocation loop radii and their concentrations the good fit of both RCs in the whole measured angular ranges including the total reflection ranges has been obtained. However, the sets of dislocation loop characteristics determined for two reflections independently were remarkably different. After introducing third radius and concentration of dislocation loops as fit parameters, the practically full coincidence of the sets of the characteristics has been achieved for two reflections with good values of normal (R) and weighted (R_w) reliability factors (see Table I and Fig. 5).

The important factor for the successful fit procedure was the self-consistency of the RC description in the total reflection range (at the Bragg peak) and at RC tails. Particularly, as can be seen in Figs. 3(b) and 4(b), the contribution of DS intensity from dislocation loops is suppressed due to extinction effect in the total reflection range for (111) reflection [Fig. 3(b)] and its influence here is small, whereas for (333) reflection the contributions of diffuse and coherent components are comparable in this region despite the extinction effect [Fig. 4(b)]. It should be emphasized that the dislocation loop characteristics determined for two reflections independently are quite close, which can be considered as the evidence for the reliability of the performed x-ray characterization.

On the other hand, the high sensitivity of RC diffuse components to effective radii of microdefects provides the possibility to characterize the complicated defect structures consisting of several microdefect types. Such kind complicated defect structures are often encountered in thermally treated Cz Si crystals.[45] The reliable characterization of various-type microdefects present in a single crystal simultaneously can be achieved due to qualitatively different behavior of DS intensity profiles in different angular intervals for microdefects with significantly different effective radii, which cause mutual shifts of corresponding boundaries between Huang and Stockes-Wilson scattering regions.

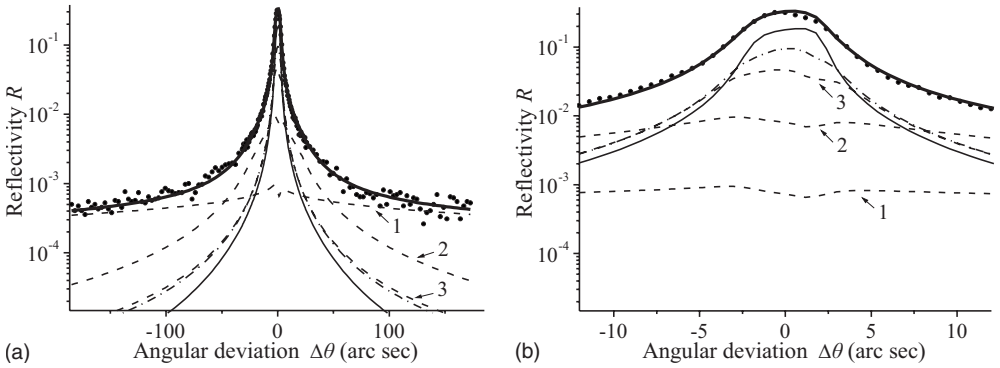

FIG. 7. See caption to Fig. 6, reflection Si (333).

TABLE II. Characteristics of perfect dislocation loops and oxygen precipitates in Cz Si sample.

hkl	*i* [a]	R_C (nm)	h_C (nm)	n_C (cm^{-3})	R_L (nm)	n_L (cm^{-3})	R (%)	R_w (%)
111	1	3	6	3.4×10^{16}	600	5.0×10^{9}	9	12
	2	70	5	2.0×10^{11}				
	3	500	11	6.5×10^{8}				
333	1	3	6	1.7×10^{16}	400	2.5×10^{10}	6	13
	2	150	7	1.0×10^{10}				
	3	600	12	2.0×10^{8}				

[a] i numerates different populations of oxygen precipitates.

For the detailed quantitative characterization of microdefects in Cz Si crystal, one should choose the appropriate model of defect structure. It is well known that in the Cz Si crystal oxygen precipitates grow during anneals at elevated temperatures.[45] The high stress at the interface between the silicon matrix and new phase particles SiO_x is released via emission of interstitial silicon atoms, which agglomerate into dislocation loops and stacking faults.[46–49] For this reason, in the defect model which was used to treat the measured RCs from Cz Si sample (Figs. 6 and 7), the simultaneous presence of two types of microdefects was supposed, namely, ellipsoidal and spherical oxygen precipitates[50] with a radius R_C and thickness h_C, and circular dislocation loops $\langle 110\rangle$ with a radius R_L, both randomly distributed without mutual correlation.

As can be seen from fitted RCs in Figs. 6 and 7 with all the DS intensity components shown, indeed the significant shift of boundaries between Huang and Stockes-Wilson scattering regions for oxygen precipitates and dislocation loops exists for both reflections measured, and these boundaries are defined sufficiently well, thus, providing the reliable quantitative determination of defect characteristics. Similarly to the previous case considered, also here an additional factor providing the unambiguity of the defect characterization was the self-consistency of the description of RC components at tails and in the total reflection range [Figs. 6(b) and 7(b)]. The obtained characterization results are given in Table II and are close for two reflections as well.

In conclusion, it should be emphasized that the additional important factor for the reliability of defect characterization in both FZ Si and Cz Si samples, besides the differences in effective radii of microdefects, was the self-consistent account for the absorption due to DS in the coherent components of RCs. The importance of accounting for both contribution of thermal DS and influence of the instrumental factors of DCD to avoid systematical errors when determining microdefect characteristics by using measured RCs should be noted as well.

VII. RESUME AND CONCLUSIONS

The theoretical diffraction model has been proposed for the self-consistent description of coherent and diffuse components of RCs measured by DCD with widely open detector window from crystals, which contain randomly distributed microdefects of several types simultaneously. The model is based on the generalized dynamical theory of x-ray scattering by imperfect single crystals with microdefects of arbitrary sizes, and the derived analytical expressions for coherent and DS intensities take account for both contribution of thermal DS and influence of instrumental factors of DCD, including the acceptance aperture of detector window.

The diagnostic possibilities of the developed model have been demonstrated as applied to the quantitative characterization of complicated defect structures in the silicon single crystals grown by floating zone and Czochralsky methods. In the investigated FZ Si single crystal, the number densities of dislocation loops with a wide spread of sizes ranged from nanometers to micrometers have been determined by using RCs measured for two reflections of the characteristic Cu K_α radiation. The characterization results of the annealed Cz Si single crystal include concentrations and radii of oxygen precipitates and dislocation loops present in the crystal simultaneously.

In whole, the obtained characterization results show that the developed analytic diffractometric model allows, at the proper choice of microdefect models, to perform reliable determination of the quantitative statistical characteristics of complicated microdefect structures in real single crystals by using high-resolution DCD measurements.

[1] J. E. Thomas, T. O. Baldwin, and P. H. Dederichs, Phys. Rev. B **3**, 1167 (1971).
[2] B. C. Larson and W. G. Schmatz, Phys. Rev. B **10**, 2307 (1974).
[3] P. Ehrhart and W. Schilling, Phys. Rev. B **8**, 2604 (1973).
[4] P. Ehrhart and U. Schlagheck, J. Phys. F: Met. Phys. **4**, 1575 (1974).
[5] H. Peisl, J. Appl. Crystallogr. **8**, 143 (1975).
[6] B. C. Larson, J. Appl. Crystallogr. **8**, 150 (1975).
[7] R. S. Averback and P. Ehrhart, J. Phys. F: Met. Phys. **14**, 1347 (1984).

[8] U. Schubert, H. Metzger, and J. Peisl, J. Phys. F: Met. Phys. **14**, 2457 (1984).
[9] B. C. Larson and F. W. Young, Phys. Status Solidi A **104**, 273 (1987).
[10] I. Hashimoto and T. Yamazaki, Phys. Status Solidi A **147**, 45 (1995).
[11] J. R. Patel, J. Appl. Crystallogr. **8**, 186 (1975).
[12] A. N. Morozov and V. T. Bublik, J. Cryst. Growth **97**, 475 (1989).
[13] L. A. Charniy, A. N. Morozov, V. T. Bublik, K. D. Scherbachev, I. V. Stepantsova, and V. M. Kaganer, J. Cryst. Growth **118**, 163 (1992).
[14] P. Franzosi, J. Cryst. Growth **126**, 85 (1993).
[15] P. Ehrhart, J. Nucl. Mater. **216**, 170 (1994).
[16] R. J. Matyi, M. R. Melloch, K. Zhang, and D. L. Miller, J. Phys. D **28**, A139 (1995).
[17] K. Karsten and P. Ehrhart, Phys. Rev. B **51**, 10508 (1995).
[18] A. Pillukat, K. Karsten, and P. Ehrhart, Phys. Rev. B **53**, 7823 (1996).
[19] T. Yamazaki and I. Hashimoto, Phys. Rev. B **56**, 5228 (1997).
[20] M. A. Krivoglaz, *Diffraction of X-Rays and Thermal Neutrons in Imperfect Crystals* (Springer, Berlin, 1992).
[21] P. H. Dederichs, Phys. Rev. B **4**, 1041 (1971).
[22] P. H. Dederichs, J. Phys. F: Met. Phys. **3**, 471 (1973).
[23] P. Ehrhart, H. Trinkaus, and B. C. Larson, Phys. Rev. B **25**, 834 (1982).
[24] V. B. Molodkin, S. I. Olikhovskii, E. N. Kislovskii, and V. P. Krivitsky, A. V. Los', E. V. Pervak, G. E. Ice, and B. C. Larson, Metallofiz. Noveishie Tekhnol. **19**, 25 (1997).
[25] V. B. Molodkin, S. I. Olikhovskii, E. N. Kislovskii, and V. P. Krivitsky, E. G. Len', E. V. Pervak, G. E. Ice, and B. C. Larson, J. Phys. D **34**, A82 (2001).
[26] V. B. Molodkin, S. I. Olikhovskii, E. N. Kislovskii, E. G. Len, and E. V. Pervak, Phys. Status Solidi B **227**, 429 (2001).
[27] S. I. Olikhovskii, V. B. Molodkin, E. N. Kislovskii, E. G. Len, and E. V. Pervak, Phys. Status Solidi B **231**, 199 (2002).
[28] E. N. Kislovskii, S. I. Olikhovskii, V. B. Molodkin, V. V. Nemoshkalenko, and V. P. Krivitsky, E. G. Len', E. V. Pervak, G. E. Ice, and B. C. Larson, Phys. Status Solidi B **231**, 213 (2002).
[29] V. Holý and J. Kuběna, Phys. Status Solidi B **170**, 9 (1992).
[30] R. Bouchard, J. R. Schneider, S. Gupta, S. Messoloras, R. J. Stewart, H. Nagasawa, and W. Zulehner, J. Appl. Phys. **77**, 553 (1995).
[31] T. P. Vladimirova, R. F. Seredenko, V. B. Molodkin, S. I. Olikhovskii, and Ye. M. Kyslovskyy, Metallofiz. Noveishie Tekhnol. **29**, 711 (2007).
[32] Ye. M. Kyslovskyy, T. P. Vladimirova, S. I. Olikhovskii, V. B. Molodkin, E. V. Kochelab, and R. F. Seredenko, Phys. Status Solidi A **204**, 2591 (2007).
[33] L. I. Datsenko, V. B. Molodkin, and M. E. Osinovskii, *Dynamical Scattering of X-Rays by Real Crystals* (Nauk. Dumka, Kiev, 1988) (in Russian).
[34] S. Y. Olikhovsky, Y. M. Kyslovskyy, V. B. Molodkin, Y. G. Len, T. P. Vladimirova, and O. V. Reshetnyk, Metallofiz. Noveishie Tekhnol. **22**, 3 (2000).
[35] V. B. Molodkin, S. I. Olikhovskii, and A. N. Kostyuk, Phys. Status Solidi B **183**, 59 (1994).
[36] Ch. Kittel, *Introduction to Solid-State Physics* (Wiley, New York, 1986).
[37] R. Bubakova, J. Drahokoupil, and A. Fingerland, Czech. J. Phys., Sect. B **11**, 205 (1961).
[38] K. Godwod, Phys. Status Solidi A **2**, 235 (1970).
[39] Z. G. Pinsker, *Dynamical Scattering of X-Rays in Perfect Crystals* (Springer, Heidelberg, 1978).
[40] P. M. Petroff and A. J. R. de Kock, J. Cryst. Growth **30**, 117 (1975).
[41] H. Föll, U. Gösele, and B. O. Kolbesen, J. Cryst. Growth **52**, 907 (1981).
[42] P. J. Roksnoer and M. M. B. van der Boom, J. Cryst. Growth **53**, 563 (1981).
[43] P. J. Roksnoer, J. Cryst. Growth **68**, 596 (1984).
[44] T. Y. Tan and U. Gösele, Appl. Phys. A: Solids Surf. **37**, 1 (1985).
[45] A. Borghesi, B. Pivac, A. Sassella, and A. Stella, J. Appl. Phys. **77**, 4169 (1995).
[46] T. Y. Tan and W. K. Tice, Philos. Mag. **34**, 615 (1976).
[47] D. M. Maher, A. Staudinger, and J. R. Patel, J. Appl. Phys. **47**, 3813 (1976).
[48] J. R. Patel, K. A. Jackson, and H. Reiss, J. Appl. Phys. **48**, 5279 (1977).
[49] W. Patrick, E. Hearn, W. Westdorp, and A. Bohg, J. Appl. Phys. **50**, 7156 (1979).
[50] S. M. Hu, Appl. Phys. Lett. **48**, 115 (1986).